Smart Structures and Systems, *Vol. 17, No. 5 (2016) 709-724*
DOI: http://dx.doi.org/10.12989/sss.2016.17.5.709

Performance assessment of buildings isolated with S-FBI system under near-fault earthquakes

Osman E. Ozbulut* and Baikuntha Silwal

Department of Civil and Environmental Engineering, University of Virginia, Charlottesville, VA, USA 22904-1000

(Received July 8, 2015, Revised November 26, 2015, Accepted December 29, 2015)

Abstract. This study investigates the optimum design parameters of a superelastic friction base isolator (S-FBI) system through a multi-objective genetic algorithm to improve the performance of isolated buildings against near-fault earthquakes. The S-FBI system consists of a flat steel-PTFE sliding bearing and superelastic NiTi shape memory alloy (SMA) cables. Sliding bearing limits the transfer of shear across the isolation interface and provides damping from sliding friction. SMA cables provide restoring force capability to the isolation system together with additional damping characteristics. A three-story building is modeled with S-FBI isolation system. Multiple-objective numerical optimization that simultaneously minimizes isolation-level displacements and superstructure response is carried out with a genetic algorithm in order to optimize S-FBI system. Nonlinear time history analyses of the building with optimal S-FBI system are performed. A set of 20 near-fault ground motion records are used in numerical simulations. Results show that S-FBI system successfully control response of the buildings against near-fault earthquakes without sacrificing in isolation efficacy and producing large isolation-level deformations.

Keywords: shape memory alloys; base isolation; near-fault earthquake; seismic control; friction

1. Introduction

Over the past decades, seismic isolation has been successfully applied to buildings, bridges, and nuclear power plants to reduce the damaging effects of earthquakes and proven to be effective. Seismic isolation is based on the concept of decoupling the substructure and superstructure to prevent the transfer of the earthquake energy to superstructure. This is achieved by introducing lateral flexibility and energy absorption capability at the support-structure interface. The introduction of flexible isolation element shifts the natural period of the structure out of the dominant seismic energy.

Although the use of seismic isolation can significantly enhance the seismic performance of structures, many studies have shown that base-isolated structures can be vulnerable to near-fault ground motions (Jangid and Kelly 2001, Shen *et al*. 2004, Karalar *et al*. 2012, Ghaffarzadeh 2013). The near-fault motions are characterized with large amplitude velocity pulses and can cause large deformations at the isolation level. The large isolation displacements indicate the need for larger

*Corresponding author, Dr., E-mail: ozbulut@virginia.edu

Copyright © 2016 Techno-Press, Ltd.
http://www.techno-press.org/?journal=sss&subpage=8 ISSN: 1738-1584 (Print), 1738-1991 (Online)

size isolation devices and seismic gaps. The extensive deformations also increase the potential of impact or pounding of a structure with adjacent building (Hall 1995, Nagarajaiah 1995). It was shown that the pounding significantly affects the performance of the isolated buildings (Pant and Wijeyewickrema 2012). In addition, seismic isolators may have large residual deformations under these strong events and need to be replaced or repaired after the event.

A number of researchers have proposed different strategies to reduce large displacement response of isolated structures during near-fault earthquakes. Some researchers have suggested the use of supplemental semi-active or active dampers to provide an adaptive control force (Casciati *et al.* 2012). Etedali *et al.* (2013) and Ozbulut *et al.* (2011a) explored the performance of a piezoelectric friction damper installed into a five-story base-isolated building to provide additional damping. Nagarajaiah and Sahasrabudhe (2006) recommended a sliding isolation system with a variable stiffness device and performed analytical and experimental studies to investigate the performance of the isolation system. Agrawal *et al.* (2006) studied the effectiveness of several active control systems to mitigate the response of buildings under near-fault earthquakes. Although semi-active and active control systems can adapt the mechanical response of the isolation system to avoid adverse effects of near-fault motions, passive control strategies can be more reliable and be implemented more easily. Several passive-type isolation systems such as multiple friction pendulum isolators (Fenz and Constantinou 2008), variable-frequency rocking bearings (Lu and Hsu 2013) and sliding isolators with variable curvature (Panchal and Jangid 2008) have been developed and investigated. Recently, shape memory alloy (SMA)-based isolators have been proposed as an alternative passive base isolation system.

Shape memory alloys (SMAs) are becoming increasingly popular in structural applications because of their material properties that include a high damping capacity, fatigue resistance, durability, and re-centering ability (Ozbulut *et al.* 2011b). The two most prominent properties of SMAs are the shape memory effect, which is the ability of the material to return to its original shape after heating, and superelastic effect, which is the ability of the material to recover its large inelastic deformations upon the removal of the load. A number of researchers have explored the potential application of superelastic SMAs in a seismic isolation system (Casciati *et al.* 2007, Jalali *et al.* 2011, Casciati and Hamdaoui 2008, Casciati and Faravelli 2009, Dezfuli and Alam 2013). Attanasi *et al.* (2009) conducted an analytical study to investigate the feasibility of isolation systems with SMAs. They found that an isolation system that relies solely on SMAs for energy dissipation provides less favorable seismic performance than isolation system with bilinear force-deformation characteristics. Therefore, SMA-based Rubber Bearing (SRB) systems that combine SMAs with rubber bearings (Ozbulut and Hurlebaus 2011c, Bhuiyan and Alam 2013) and Superelastic-Friction Base Isolator (S-FBI) systems that consist of steel-Teflon flat sliding bearing and superelastic SMAs (Ozbulut and Hurlebaus 2010a, 2012, Gur *et al.* 2014) have been examined. In a comparative study, Ozbulut and Hurlebaus (2011d) carried out an energy-based performance assessment of the SRB systems and S-FBI systems and found that S-FBI system shows better structural performance while requiring significantly less SMA material.

This study explores optimal design parameters for S-FBI systems that enhance the performance of buildings under near-fault earthquakes. In what follows, the design and behavior of the S-FBI system are discussed first. Then, a multi-objective genetic algorithm is employed to optimize the S-FBI system parameters. A three-story steel frame building is modeled for numerical investigations. Next, extensive nonlinear response history analyses are performed to assess the effectiveness of the S-FBI system. The simulations of the fixed-base building are also conducted to serve as benchmark. Finally, the simulation results are discussed in terms of peak and residual

isolation displacements, peak interstory drifts and peak floor accelerations.

2. Superelastic friction base isolation systems

An S-FBI system combines a flat-sliding bearing and SMA elements. Flat-sliding bearings consist of a stainless steel plate that moves across a PTFE layer and dissipate energy through friction while providing rigidity under gravity loads. By using lubricated or non-lubricated sliding material, a variety of coefficient of frictions can be obtained based on design requirements. SMA elements are mainly employed to provide additional damping and improve re-centering properties, and thereby reduce the residual isolator deformations. SMA elements can be implemented as an auxiliary device or as a single unit with the sliding bearings.

Shape memory alloy cables have been recently developed as an alternative and new structural element (Daghash *et al.* 2014, Ozbulut *et al.* 2015). They leverage the superior mechanical characteristics of small diameter SMAs into large-size structural tension elements. Besides, they have considerable cost advantages over same size monolithic SMA bars (Reedlunn *et al.* 2013). Fig. 1 presents schematic drawing of the cross-section of an NiTi SMA cable that has a $7 \times 7 \times 0.885$ mm design and its longitudinal section.

(a) (b)

Fig. 1 Shape memory cable: cross-sectional and longitudinal views

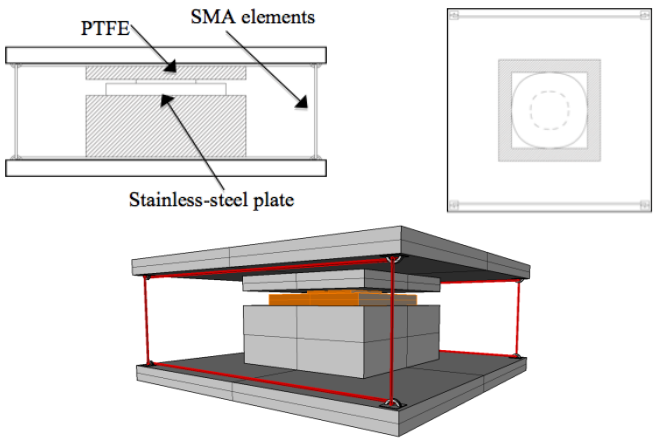

Fig. 2 Superelastic-friction base isolator

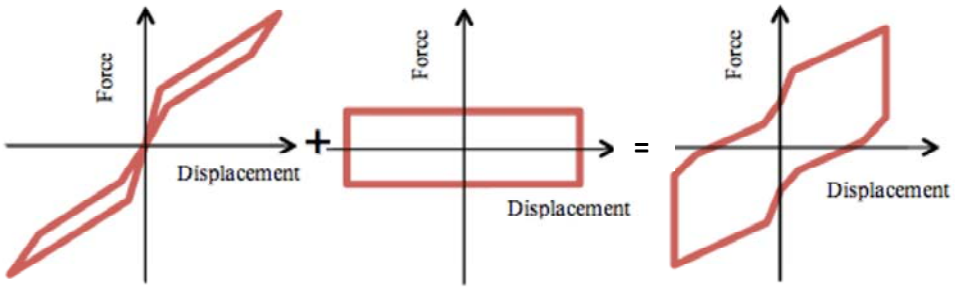

Fig. 3 Idealized force displacement curves of S-FBI system and its subcomponents

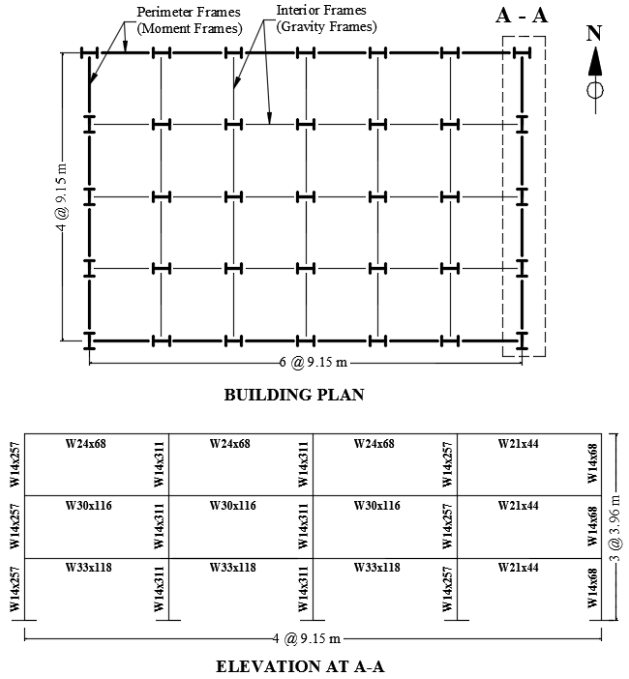

Fig. 3 Idealized force displacement curves of S-FBI system and its subcomponents

The SMA cables can be used as the SMA elements of the S-FBI system. Here, the SMA cables are wrapped around low-friction wheels attached at each corner of the top and bottom cover plates to obtain a compact isolator as shown in Fig. 2. Whether the isolation system itself moves left or right, the configuration ensures that the SMA elements will remain under tension. No pre-tensioning force was assumed in the SMA elements.

The mechanical response of the S-FBI system features a flag-shaped hysteresis curve as shown in Fig. 3. By changing the design parameters of the sliding bearing (coefficient of friction, μ) and SMA elements (cross-sectional area and length of SMAs), the energy dissipation and re-centering ability of the S-FBI system can be altered.

3. Three-story benchmark steel building

A three-story steel building is selected to assess the performance of the S-FBI systems. This building has served as a benchmark structure for nonlinear seismic control design and was developed for the SAC Phase II Steel Project (Ohtori *et al.* 2004). The building is 36.6 m by 54.9 m in plan, and 11.9 m in elevation. The building consists of four bays at 9.15 m in the north-south (N-S) direction and six bays at 9.15 m in the east-west (E-W) direction. The story height is 3.96 m at each floor as shown in Fig. 4. The floor system consists of 248 MPa steel wide flange beams acting compositely with the floor slab and is assumed to be rigid in the horizontal plane. The columns are 345 MPa steel and modeled as fixed to the ground. The seismic masses of the first and second levels are 9.57×10^5 kg, and the mass of the third level is 1.04×10^6 kg. The fundamental period of the structure is 1.01 second. The special steel moment-resisting frames on the perimeter of the building provide the lateral load resistance for the structure. One of the perimeter steel special moment frames in the N-S direction is considered for numerical simulations in this study. One-half of the seismic mass associated with the entire building is assigned to the perimeter frame since the inertial effects of each level are evenly transferred by the floor diagram to each perimeter frame.

4. Multi-objective optimization of S-FBI system parameters

Genetic algorithm (GA) is a search technique that emulates biological evolutionary theories for optimization and search. The method has been successfully applied to solving a wide range of optimization problems. In order to determine the optimal design parameters for S-FBI system, a non-dominated multi-objective algorithm (NSGA-II) is employed for optimization. NSGA-II is a computationally fast and elitist evolutionary algorithm based on a non-dominated sorting approach. Among a pool of initial random candidate values that reside within a user-defined range, NSGA-II generates a set of Pareto-optimal solutions through an iterative process. In particular, it compares each solution with every other solution in the population to determine if it is dominated, and then evaluates the solutions in accordance with given performance objectives. The detailed description of NSGA-II algorithm can be found in Deb *et al.* (2002). Here, a total of three variables, that are, the friction coefficient of sliding bearing (μ), the yield displacement of SMA elements (u_y^{SMA}), and the total yield strength of SMA elements normalized by the total weight of the structure (F_o), are adjusted to find an optimal solution using NSGA-II. The specified ranges for the design parameters μ, u_y^{SMA} (in millimeters), and F_o are [0.03, 0.15], [60, 120], and [0.03, 0.15], respectively.

For evaluation of candidate solutions during NSGA-II optimization, a seismic excitation is required. Using only a near-fault ground motion record during optimization may lead to a relatively stiff isolation system during far-fault earthquakes, which might eliminate the isolation effectiveness. Since here the goal is to have an isolation system that is effective against both far-fault and near-fault earthquakes, 1994 Northridge (Beverly Hills station) and 1979 Imperial Valley (El-Centro Array #6 station) records, employed also in FEMA P695 (FEMA 2009), are used to represent far-fault and near-fault excitations respectively during GA simulations. In order to evaluate each chromosome, four objective functions are defined as follows

$$J_1 = \frac{\max_{t\,(NF)} \left\| x_f(t) \right\|}{\max_{t\,(NF)} \left\| \hat{x}_f(t) \right\|} \quad J_2 = \frac{\max_{t\,(FF)} \left\| \ddot{x}_f(t) \right\|}{\max_{t\,(FF)} \left\| \hat{\ddot{x}}_f(t) \right\|}$$
$$J_3 = \frac{\max_{t\,(NF)} \left\| x_b(t) \right\|}{(x_{b,d})_{\max}} \quad J_4 = \frac{x_y^{SMA}}{\max_{t\,(NF)} \left\| x^{SMA}(t) \right\|} \tag{1}$$

where $\hat{x}_f$ and x_f denote interstory drift for fixed-base and isolated buildings, respectively; and $\hat{\ddot{x}}_f$ and $\ddot{x}_f$ are absolute floor acceleration for fixed-base and isolated buildings, respectively; t is time; and f represents the story that is considered; x_b is the isolator displacement; $(x_{b,d})_{\max}$ is the maximum design isolator displacement; x^{SMA} is the yield displacement of SMAs; and x_y^{SMA} is the yield displacement of SMAs. The objective function J_1 evaluates peak interstory drift in the isolated structure normalized by corresponding displacement in the fixed-base structure during the near-fault (NF) earthquake. On the other hand, the objective function J_2 evaluates peak absolute floor acceleration in the isolated building normalized by corresponding acceleration in the fixed-base structure during the far-fault (FF) earthquake. The objective functions J_3 and J_4 are related to the response of isolation system under the near-fault earthquake. The objective function J_3 computes the peak displacement of the S-FBI system normalized by the maximum design isolator displacement, which is selected as 60 cm. The objective function J_4 evaluates the ratio of yield displacement of SMA elements of the S-FBI system to maximum displacement of the S-FBI system. A lower value of J_4 indicates more energy dissipation for SMA elements as can be seen from Fig. 5. This evaluation criterion is defined to ensure that the SMA elements of the S-FBI system will experience large enough strain to dissipate energy with the selected design parameters.

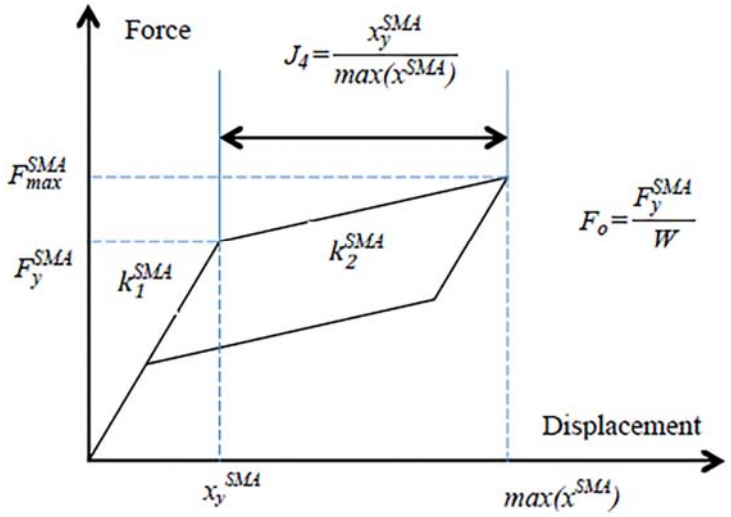

Fig. 5 Design parameters for SMA elements

In order to reduce the computational effort during the optimization, a lumped-mass structure model with one degree of freedom per floor is used in the numerical simulations. The lateral stiffness of each floor is selected to be k_1= 590644.7, k_2= 61701.3, and k_3= 43940.4 kN/m. These values were determined by minimizing the difference between the frequencies and the mode shapes of a condensed and a shear-type model of the three-story benchmark building in a previous study (Cimellaro 2008). The damping matrix is computed by assuming 2% Rayleigh damping on the first two modes. A neuro-fuzzy model developed by Ozbulut and Hurlebaus (2010b) is used to capture the response of the SMAs employed in the S-FBI system. The Coulomb-friction model is used to simulate the mechanical response of the sliding bearings. The MATLAB (2013) is used to implement the NSGA-II algorithm and to obtain the dynamic response of the isolated building for the optimization. With above-described settings, a population of 50 chromosomes is initialized for a total of 100 GA runs. Four objective functions from the response of the structure are measured simultaneously and organized into a set of Pareto fronts.

5. Nonlinear dynamic analyses

In this section, nonlinear response history analyses of the fixed-base and isolated buildings with a set of 20 historical near-fault ground motion records are performed. The optimum design parameters of the S-FBI system that effectively mitigate the response of the 3-story benchmark building is determined to be μ=0.10 , $u_y^{SMA} = 70\,\text{mm}$, and $F_o = 0.05$ by NSGA-II optimization. To explore the performance of the optimal S-FBI system, detailed finite element models of the benchmark building and the S-FBI system are constructed.

5.1 Modelling benchmark building

OpenSees (2013), a finite element framework for nonlinear and dynamic analysis of structural systems, is used to model the benchmark structure as fixed-base and as isolated with S-FBI system. The plane frame elements of the structure are modeled with *nonlinearBeamColumn* element, which considers the spread of plasticity along the element. To define element cross-section in OpenSees, fiber section approach was utilized to represent wide flange steel sections for beam and column elements. The *steel01* material is assigned to structural elements to represent the bilinear hysteresis model. Since the lateral load-resisting system is composed of two MRFs on the exterior frames, each exterior frame is assumed to carry one half of seismic mass.

In a building structure, when an individual story experience a lateral deflection (referred as Δ) under applied horizontal loads, the resulting eccentricity of the gravity loading (referred as P) from the inclined axes of the structure's vertical members causes an increase in the deflections and moments. This second-order effect is known as P-Δ effect. To consider the P-Δ effects, leaning columns are connected to the plane frame with rigid links to experience the same lateral deformation at each story level. For leaning columns, *elasticBeamColumn* elements with large axial and bending stiffness are used. The hinges with low rotational stiffness are introduced as zero length elements at the ends of the element. Rigid links that connect the frame and the leaning column at each story level are modeled using a truss element with high axial stiffness. The gravity loads tributary to the perimeter frame are applied to the beams of the perimeter frame as a combination of distributed load and point load. Since a 2D model is used and only the perimeter frame is modeled, the gravity loading carried by the interior frames is applied to the leaning

columns as point load.

5.2 Modeling S-FBI system

The superelastic-friction base isolator is modeled using a friction element and a self-centering element in parallel. In particular, a *flatSliderBearing* element with zero-length is used to simulate the sliding bearings and a zero-length element with uniaxial self-centering material is employed to capture the behavior of SMAs. The properties of the self-centering material are assigned in accordance with the properties of the SMAs. These properties are obtained from the experimental tests conducted on NiTi SMAs by Ozbulut and Hurlebaus (2010b) and discussed below. Note that no degradation in the cyclic response of the SMAs is considered in this study. An in-depth discussion on the fatigue performance of SMAs can be found in Carreras *et al.* (2011) and Torra *et al.* (2013).

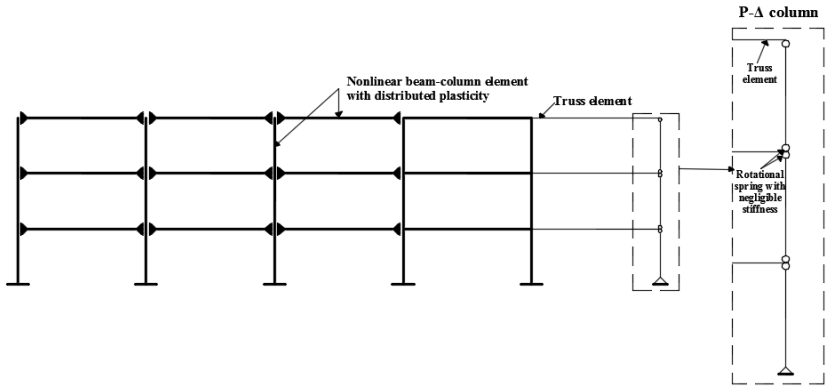

Fig. 6 Analytical model of three story benchmark building

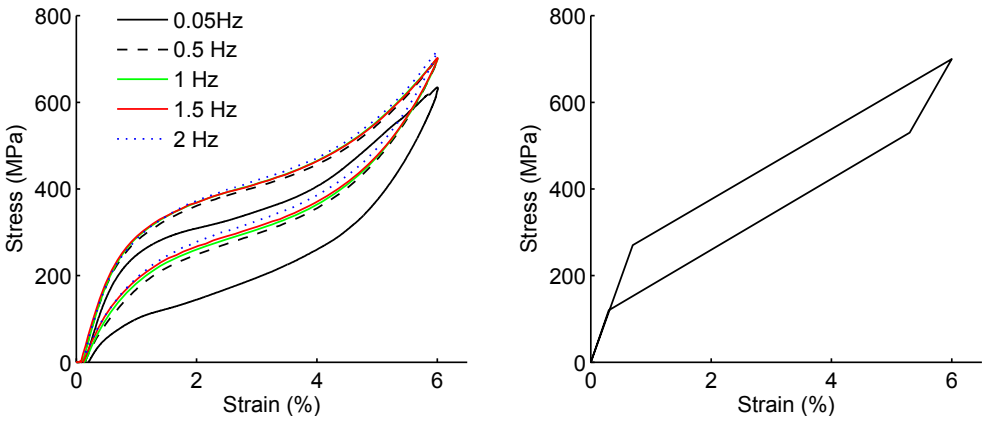

Fig. 7 (a) Experimental stress-strain behavior of SMAs at various loading frequencies and (b) simplified model

Table 1 Characteristics of the near-fault ground motions used in the analyses

SAC Name	Earthquake	Component	Magnitude (M_w)	Distance (km)	Peak Ground Acceleration (g)
NF01	Tabas, 1978	Fault-Normal	7.4	1.2	0.90
NF02	Tabas, 1978	Fault-Parallel	7.4	1.2	0.98
NF03	Loma Prieta, 1989, Los Gatos	Fault-Normal	7.0	3.5	0.72
NF04	Loma Prieta, 1989, Los Gatos	Fault-Parallel	7.0	3.5	0.46
NF05	Loma Prieta, 1989, Lex. Dam	Fault-Normal	7.0	6.3	0.69
NF06	Loma Prieta, 1989, Lex. Dam	Fault-Parallel	7.0	6.3	0.37
NF07	C. Mendocino, 1992, Petrolia	Fault-Normal	7.1	8.5	0.64
NF08	C. Mendocino, 1992, Petrolia	Fault-Parallel	7.1	8.5	0.66
NF09	Erzincan, 1992	Fault-Normal	6.7	2.0	0.43
NF10	Erzincan, 1992	Fault-Parallel	6.7	2.0	0.46
NF11	Landers, 1992	Fault-Normal	7.3	1.1	0.71
NF12	Landers, 1992	Fault-Parallel	7.3	1.1	0.8
NF13	Nothridge, 1994, Rinaldi	Fault-Normal	6.7	7.5	0.89
NF14	Nothridge, 1994, Rinaldi	Fault-Parallel	6.7	7.5	0.39
NF15	Nothridge, 1994, Olive View	Fault-Normal	6.7	6.4	0.73
NF16	Nothridge, 1994, Olive View	Fault-Parallel	6.7	6.4	0.60
NF17	Kobe, 1995	Fault-Normal	6.9	3.4	1.09
NF18	Kobe, 1995	Fault-Parallel	6.9	3.4	0.58
NF19	Kobe, 1995, Takatori	Fault-Normal	6.9	4.3	0.79
NF20	Kobe, 1995, Takatori	Fault-Parallel	6.9	4.3	0.42

Previous experimental studies on the NiTi SMAs have revealed that the loading frequency affects the mechanical response of SMAs. However, when the loading frequency is changed between 0.5-2 Hz, the hysteresis loops are almost stable (see Fig. 7). Since the SMAs will be subjected to dynamic loading rates during a seismic event, the material parameters for the SMA elements considered in this study are selected to match experimental response of SMAs at high loading frequencies. In particular, the SMA elements are assigned to have a modulus of elasticity of 38.6 GPa and a forward transformation stress of 270 MPa. The initial stiffness and post-transformation stiffness, shown as k_1^{SMA} and k_2^{SMA} in Fig. 5, are set to be 2802.7 kN/m and 502.9 kN/m, respectively.

5.3 Ground motions

A total of 20 ground motion records that are used in SAC Steel Project (Somerville *et al.* 1997) are employed as external excitation in the numerical simulations. The records are derived from fault-normal and fault-parallel orientations of 10 historical earthquakes. The characteristics of selected ground motions are given in Table 1.

6. Results

Structural responses of non-isolated and isolated structures are computed under each ground motion record. As the distribution of seismic response is typically assumed to follow a lognormal distribution, the statistics of the peak interstory drift ratio, which is defined as the ratio of the relative displacement of a particular floor to the story height at that level, and peak story absolute acceleration response under 20 near-fault ground motion records are provided in terms of median (50 percentile) and 84 percentile response and calculated as

$$\hat{X} = \exp\left(\frac{\sum_{i=1}^{n} \ln x_i}{n}\right) \tag{2}$$

$$X^{84} = \hat{X} \exp\left(\sigma_{\ln x_i}\right) \tag{3}$$

where n is the number of response data points and $\sigma_{\ln X}$ is the standard deviation of the logarithm of response X. Fig. 8 show the median and the 84th percentile values of the peak interstory drift ratios and peak story accelerations at each floor level for the fixed-base and isolated buildings. It can be seen that when the three-story building is isolated with the S-FBI systems, story drifts are considerably reduced as compared to non-isolated structure under near-fault earthquakes. In particular, the median peak interstory drift is decreased from 3.2% for the fixed building to 1.5% for the isolated building. It can be also seen that the dispersion of story drift ratio is higher for the non-isolated building. Note that although the superior performance of the isolated buildings under design event is generally expected, drift demands in the isolated structures can be larger than in a fixed-base building under strong events (FEMA 2009). The S-FBI system also effectively limits the peak floor accelerations. Peak story acceleration demand in the isolated building is reduced about 64% relative to fixed-base building.

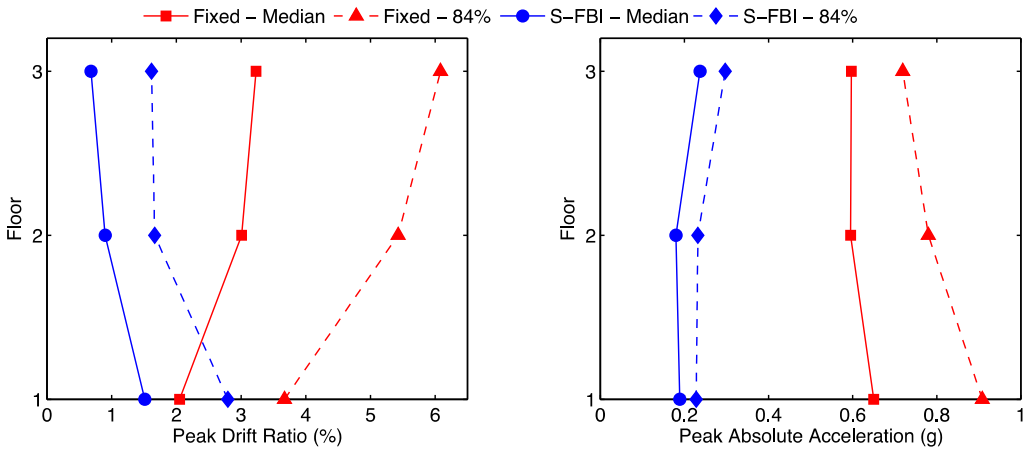

Fig. 8 Profiles of peak interstory drift ratio and peak story absolute acceleration for non-isolated building and S-FBI systems

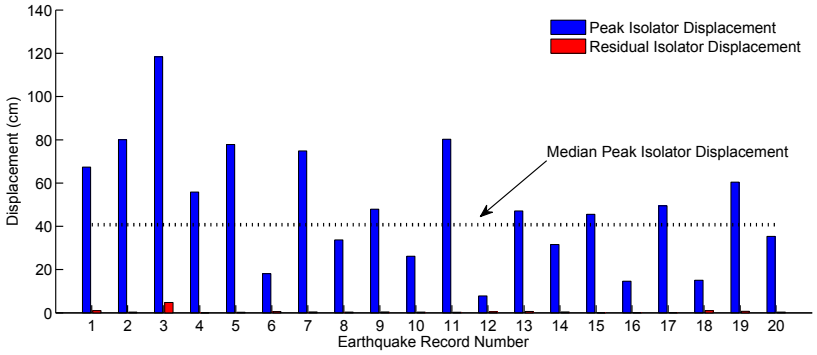

Fig. 9 Peak and residual isolator displacement for S-FBI system under each ground motion

The peak and residual isolator displacements under each ground motion are given in Fig. 9. The median peak isolator displacement for the S-FBI system is found to be 40.7 cm. The residual isolator displacement of S-FBI system is below 1 cm for most of the excitation cases. The S-FBI system was able to recover its deformations even for the earthquakes where extensive isolation deformations are observed. That indicates very good re-centering capability of the SFBI systems even under near-fault earthquakes.

The time histories of various response quantities under NF01 ground motion record are examined next. The acceleration time history and corresponding Power spectrum of NF01 record are given in Fig. 10. Fig. 11 shows the response history of the isolator displacement to NF01 record. A large pulse with displacement response up to 62 cm is noticed. It can be also seen that the isolation system recovers its deformations at the end of ground motion.

Force-deformation curves of the S-FBI system and its subcomponents, i.e., the SMA elements and the sliding bearing are given in Fig. 12. The total response of S-FBI system resembles a double flag-shaped hysteresis, which indicates the re-centering capacity of the isolation system. The amount of the energy dissipated by the SMA elements and PTFE sliding bearing are shown in Fig. 13 together with the total dissipated energy. It can be seen that the sliding bearing component of the S-FBI system absorbs a large part of the seismic energy, while the SMA elements modestly contribute to the energy dissipation through their hysteretic behavior.

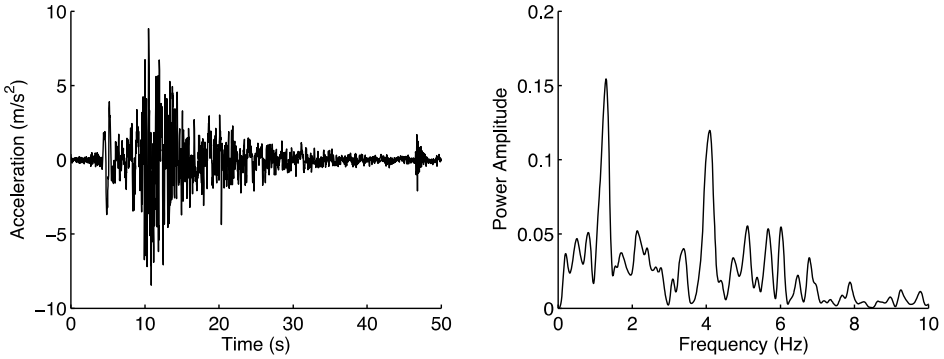

Fig. 10 Acceleration time history and corresponding Power spectrum of NF01 record

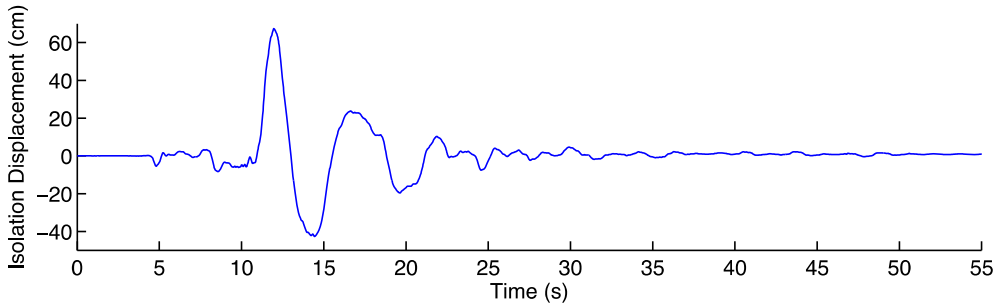

Fig. 11 Time history of S-FBI system displacement under NF01 record

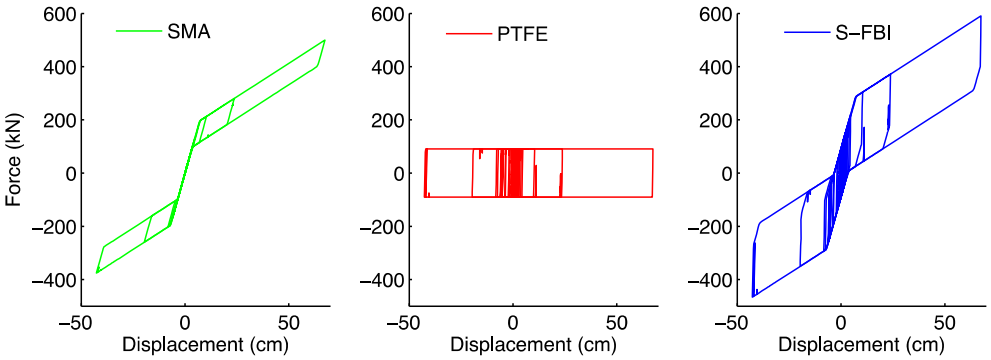

Fig. 12 Force-deformation curves of S-FBI system and its subcomponents under NF01 record

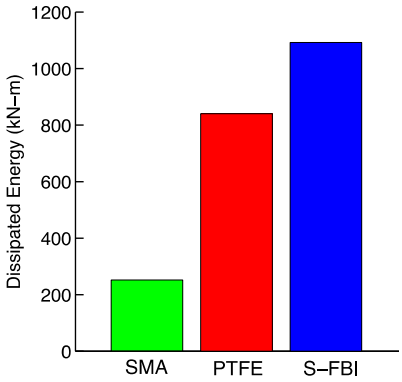

Fig. 13 Energy dissipated by the S-FBI system and its subcomponents under NF01 record

Typical time histories of the top floor absolute acceleration and top floor drift under NF01 ground motion record for the fixed-base and isolated buildings are shown in Fig. 14. It can be

noticed that the peak top floor drift is significantly reduced for the isolated building as compared to the fixed-base building, which also possessed some permanent drifts at the end of seismic event. From time-histories of the acceleration response, it can be seen that the maximum values of the top floor acceleration for both fixed-base and isolated buildings are similar. Fig. 15 shows the Power spectra and the spectrograms of the top floor acceleration for the fixed-base and isolated buildings. For the fixed-base building, the peak response is observed at around 1 Hz, which also corresponds to fundamental frequency of the building.

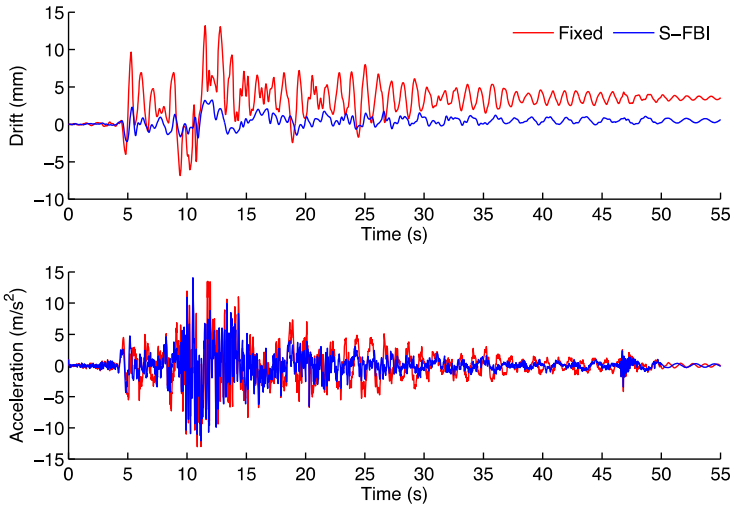

Fig. 14 Time histories of top floor drift and absolute acceleration for fixed-base and isolated structures under NF01 record

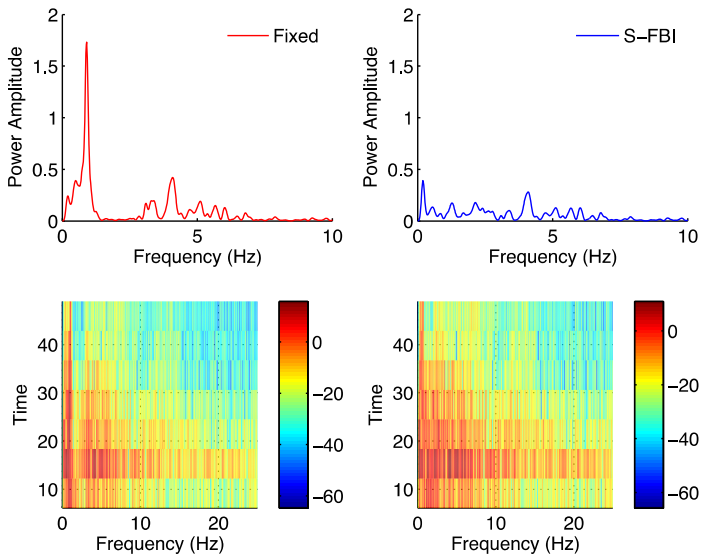

Fig. 15 Power spectrum of top floor acceleration and corresponding spectrograms for fixed-base and isolated structures under NF01 record

The peak for the isolated building is observed at lower frequencies due to the increased period of the structure. However, the Power amplitudes are significantly decreased for the isolated building. Although the transference of high frequency components of the ground motions to the floor accelerations is a concern for the isolated buildings due to their flexibility, it can be seen that the S-FBI system also reduces the response of building to the high-frequency components of the ground motion record. From the spectrograms, it can be seen that for both structures the peak response is observed around 10-15 seconds, when the ground acceleration has its maximum values.

7. Conclusions

This study aims to explore the effectiveness of S-FBI isolation system in mitigating response of buildings against near-fault earthquakes. To this end, a multi-objective genetic algorithm is first employed to determine the optimal parameters of S-FBI systems. Then, seismic assessment of a building isolated with optimal S-FBI system is performed under near-fault earthquakes. In particular, a three-story benchmark structure is modeled in OpenSees as fixed-base and isolated with S-FBI system. A suite of 20 historical near-fault ground motion records is selected for numerical investigations. Nonlinear response history analyses are conducted and the median and 84th percentile response quantities are evaluated. Results show that seismic response of the buildings can significantly reduced as compared to conventional buildings under near-fault earthquakes using S-FBI isolation system. It is also shown that S-FBI system can successfully recover its deformation upon the end of the seismic event.

References

Agrawal, A., Xu, Z. and He, W.L. (2006), "Ground motion pulse-based active control of a linear base isolated benchmark building", *Struct. Control Health Monit.*, **13**, 792-808.

Attanasi, G., Auricchio, F. and Fenves, G. L. (2009), "Feasibility assessment of an innovative isolation bearing system with shape memory alloys", *J. Earthq. Eng.*, **13**(1), 18-39.

Bhuiyan, R.A. and Alam, M.S. (2013), "Seismic performance assessment of highway bridges equipped with superelastic shape memory alloy-based laminated rubber isolation bearing", *Eng. Struct.*, **49**, 396-407.

Carreras, G., Casciati, F., Casciati, S., Isalgue, A., Marzi, A. and Torra, V. (2011), "Fatigue laboratory tests toward the design of SMA portico-braces", *Smart Struct. Syst.*, **7**(1), 41-57.

Casciati, F., Rodellar, J. and Yildirim, U. (2012), "Active and semi-active control of structures–theory and applications: A review of recent advances", *J. Intel. Mat. Syst. Str.*, **23**(11), 1181-1195.

Casciati, F. and Hamdaoui, K. (2008), "Modelling the uncertainty in the response of a base isolator", *Probabilist. Eng. Mech.*, **23**(4), 427-437.

Casciati, F. and Faravelli, L. (2009), "A Passive control device with SMA components: From the prototype to the model", *Struct. Control Health Monit.*, **16**,751-765.

Casciati, F., Faravelli, L. and Hamdaoui, K. (2007), "Performance of a base isolator with shape memory alloy bars", *Earthq. Eng. Eng. Vib.*, **6**(4), 401-408.

Cimellaro, G.P. *(*2008), "Improving seismic resilience of structural systems through integrated design of smart structures", *Ph.D. Dissertation, University at Buffalo, The State University of New York.*

Daghash, S., Ozbulut, O.E. and Sherif, M. (2014), "Shape memory alloy cables for civil infrastructure systems", *Proceedings of the ASME 2014: Smart Mate Adaptive Struct Intell Syst, SMASIS2014-7562*, Newport, RI, September.

Deb, K., Pratap, A., Agrawal, S. and Meyarivan, T. (2002), "A fast elitist non-dominated sorting genetic algorithm for multi-objective optimization: NSGA-II", *IEEE Trans. Evol. Comput*., **6**(2),182-197.
Dezfuli, F.H. and Alam, M.S. (2013), "Shape memory alloy wire-based smart natural rubber bearing", *Smart Mater. Struct.*, **22**(4), 045013.
Etedali, S., Sohrabi, M.R. and Tavakoli, S. (2013), "Optimal PD/PID control of smart base isolated buildings equipped with piezoelectric friction dampers", *Earthq. Eng. Eng. Vib.*, **12**(1), 39-54.
FEMA (2009), "*Quantification of Building Seismic Performance Factors*", Report No. P695, Federal Emergency Management Agency, Washington, D.C.
Fenz, D.M. and Constantinou, M.C. (2008), "Spherical sliding isolation bearings with adaptive behavior: Theory", *Earthq. Eng. Struct. D.*, **37**(2), 163-183.
Ghaffarzadeh, H. (2013), "Semi-active structural fuzzy control with MR dampers subjected to near-fault ground motions having forward directivity and fling step", *Smart Struct. Syst.*, **12**(6), 595-617.
Gur, S., Mishra, S.K. and Chakraborty. S. (2014), "Performance assessment of buildings isolated by shape-memory-alloy rubber bearing: Comparison with elastomeric bearing under near-fault earthquakes", *Struct. Control Health Monit.*, DOI: 10.1002/stc.1576.
Hall, J.F. (1995), "Near source ground motion and its effects on flexible buildings", *Earthq. Spectra*, **11**, 569-605.
Jalali, A., Cardone, D. and Narjabadifam, P. (2011), "Smart restorable sliding base isolation system", *Bull. Earthq. Eng.*, **9**(2), 657-673.
Jangid, R.S. and Kelly, J.M. (2001), "Base isolation for near fault motions", *Earthq. Eng. Struct. D.*, **30**, 123-131.
Karalar, M., Padgett, J.E. and Dicleli, M. (2012), "Parametric analysis of optimum isolator properties for bridges susceptible to near-fault ground motions", *Eng. Struct.*, **40**, 276-287.
Lu, L.Y. and Hsu, C.C. (2013), "Experimental study of variable-frequency rocking bearings for near-fault seismic isolation", *Eng. Struct.*, **46**, 116-129.
Math Works Inc. (2013), MATLAB R2013a, Natick, MA.
Nagarajaiah, S. (1995), "Base-isolated FCC Building: Impact response during Northridge earthquake", *J. Struct. Eng. - ASCE*, **127**(9), 1063-1074.
Nagarajaiah, S. and Sahasrabudhe, S. (2006), "Seismic response control of smart sliding isolated buildings using variable stiffness systems: an experimental and numerical study", *Earthq. Eng. Struct. D.*, **35**(2), 177-197.
Ohtori, Y., Christenson, R.E., Spencer Jr, B.F. and Dyke, S.J. (2004), "Benchmark control problems for seismically excited nonlinear buildings." *J. Eng. Mech. - ASCE*, **130**(4), 366-385.
OpenSees (2013), "The Open System for Earthquake Engineering Simulation." *http://opensees.berkeley.edu* Pacific Earthquake Engineering Research Center (PEER).
Ozbulut, O.E. and Hurlebaus, S. (2010a), "Evaluation of the performance of a sliding-type base isolation system with a NiTi shape memory alloy device considering temperature effects", *Eng. Struct.*, **32**, 238-249.
Ozbulut, O.E. and Hurlebaus, S. (2010b), "Neuro-fuzzy modeling of temperature- and strain-rate-dependent behavior of NiTi shape memory alloys for seismic applications", *J. Intel. Mat. Syst. Str.*, **21**, 837-849.
Ozbulut, O.E. Maryam, B. and Stefan, H. (2011a), "Adaptive control of base-isolated structures against near-field earthquakes using variable friction dampers", *Eng. Struct.*, **33**(12), 3143-3154.
Ozbulut, O.E. Hurlebaus, S. and DesRoches, R. (2011b), "Seismic response control using shape memory alloys: A review", *J. Intel. Mat. Syst. Str.*, **22**, 1531-1549
Ozbulut, O.E. and Hurlebaus, S. (2011c), "Seismic assessment of bridge structures isolated by a shape memory alloy/rubber-based isolation system", *Smart Mater. Struct.*, **20**, 015003.
Ozbulut, O.E. and Hurlebaus, S. (2011d), "Energy-balance assessment of shape memory alloy-based seismic isolation devices." *Smart Struct. Syst.*, **8**, 399-412.
Ozbulut, O.E. and Hurlebaus, S. (2012), "A comparative study on seismic performance of superelastic-friction base isolators against near-field earthquakes", *Earthq. Spectra*, **28**, 1147-1163.
Ozbulut, O.E., Daghash, S. and Sherif, M.M. (2015), "Shape memory alloy cables for structural

applications", *J. Mater. Civ. Eng*.,10.1061/(ASCE)MT.1943-5533.0001457*,* 04015176.
Panchal, V.R. and Jangid, R.S. (2008), "Variable friction pendulum system for near-fault ground motions", *Struct. Control Health Monit.*, **15**(4), 568-584.
Pant, D.R. and Wijeyewickrema, A.C. (2012), "Structural performance of a base-isolated reinforced concree building subjected to seismic pounding", *Earthq. Eng. Struct. D.*, **41**, 1709-1716.
Polucarpou, P. and Komodromos, P. (2010), "On poundings of a seismically isolated building with adjacent structures during strong earthquakes", *Earthq. Eng. Struct. D.*, **39**, 933-940.
Reedlunn, B., Daly, S. and Shaw, J. (2013), "Superelastic shape memory alloy cables: Part I–isothermal tension experiments", *Int. J. Solid Struct.*, **50**(20), 3009-3026.
Shen, J., Tsai, M.H., Chang, K.C. and Lee, G.C. (2004), "Performance of a seismically isolated bridge under near-fault earthquake ground motions", *J. Struct. Eng. - ASCE*, **30**(6), 861-868.
Somerville, P., Nancy, F., Punyamurthula, S. and Sun, J.I. (1997), "Development of ground motion time histories for Phase 2 of the FEMA/SAC steel project", SAC Background Document SAC/BD-91/04, SAC Joint Venture, Sacramento, CA.
Torra, V., Auguet, C., Isalgue, A., Carreras, G., Terriault, P. and Lovey, F.C. (2013), "Built in dampers for stayed cables in bridges via SMA. The SMARTeR-ESF project: a mesoscopic and macroscopic experimental analysis with numerical simulations", *Eng. Struct.*, **49**, 43-57.

FC